Slot-MLLM: Object-Centric Visual Tokenization for Multimodal LLM

Donghwan Chi*Korea University
zheedong@korea.ac.kr

Hyomin Kim* Korea University khmiee@korea.ac.kr Yoonjin Oh Korea University Yongjin Kim Korea University

Donghoon Lee Kakao Corp. **Daejin Jo** Korea University Kakao Corp. Jongmin Kim Kakao Corp. **Junyeob Baek** KAIST Sungjin Ahn KAIST

Sungwoong Kim[†] Korea University swkim01@korea.ac.kr

Abstract

Recently, multimodal large language models (MLLMs) have emerged as a key approach in achieving artificial general intelligence. In particular, vision-language MLLMs have been developed to generate not only text but also visual outputs from multimodal inputs. This advancement requires efficient image tokens that LLMs can process effectively both in input and output. However, existing image tokenization methods for MLLMs typically capture only global abstract concepts or uniformly segmented image patches, restricting MLLMs' capability to effectively understand or generate detailed visual content, particularly at the object level. To address this limitation, we propose an object-centric visual tokenizer based on Slot Attention specifically for MLLMs. In particular, based on the Q-Former encoder, diffusion decoder, and residual vector quantization, our proposed discretized slot tokens can encode local visual details while maintaining high-level semantics, and also align with textual data to be integrated seamlessly within a unified next-token prediction framework of LLMs. The resulting Slot-MLLM demonstrates significant performance improvements over baselines with previous visual tokenizers across various vision-language tasks that entail local detailed comprehension and generation. Notably, this work is the first demonstration of the feasibility of object-centric slot attention performed with MLLMs and in-the-wild natural images.

1 Introduction

Inspired by the success of LLMs, there has been a rise in ongoing research for multimodal large language models (MLLMs), aiming to leverage strong reasoning and generalization abilities of LLMs due to their extensive background knowledge. For developing such MLLMs, the most efficient way to incorporate non-text modalities into both the input and output of existing LLMs is to construct non-text discrete tokens and perform training, inference, and generation of text as well as non-text tokens within a unified framework identical to that of LLMs.

Recently, there have been trials for vision-language MLLMs that utilize discrete image tokens to efficiently process the image modality as a second language within a single, bilingual-like LLM

^{*}Equal contribution

[†]Corresponding author

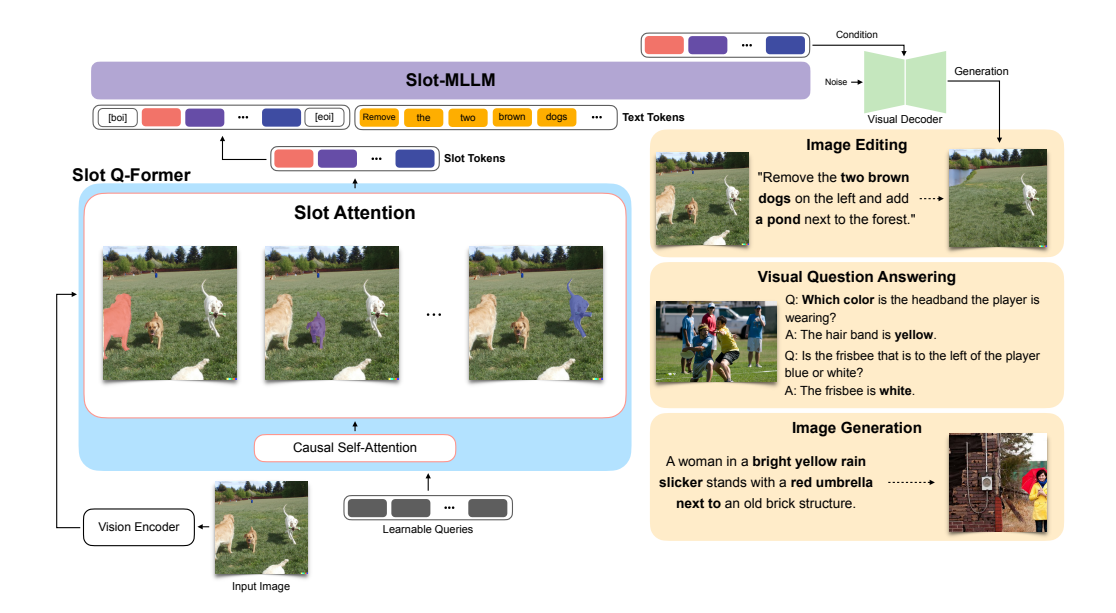


Figure 1: Overview of Slot-MLLM. Slot-MLLM employs Slot Q-Former with Slot Attention to encode images into discrete, object-centric visual tokens. These tokens are treated as a second language within the model, enabling unified autoregressive modeling across multimodal tasks such as image editing (IT2I), visual question answering (I2T), and image generation (T2I).

framework [14, 26, 74, 52, 75]. For example, in [14], an elaborate image tokenizer, called SEED, was proposed for this where causal Q-Former [37] and diffusion-based decoder [58] are used to obtain a sequence of image tokens. However, SEED tokens capture only global semantic features of the original image without maintaining the information of local details, and moreover SEED is unable to effectively distribute information across tokens representing different regions within an image. This limitation restricts the corresponding MLLM's capability in faithfully analyzing or generating local or object-level details of image content. To overcome this limitation, a number of recent works [26, 73] have tried to produce a set of local semantic tokens. However, these methods adopt some ad-hoc clustering and merging processes on top of patch-level image features.

Indeed, a well-known, more principled approach typically used to distribute object-centric features within an image is Slot Attention [44]. In this work, we propose to obtain a sequence of object-centric visual tokens for MLLMs through slot attention mechanism that generates image masks in an unsupervised manner via attention competition between queries. In specific, the sequential Q-Former is augmented with slot attention to extract a set of visual tokens from an image where each token represents a distinct region within an image, such as objects, and the modified diffusion decoder reconstructs the original image from the slot visual tokens. Here, slot tokens are discretized by residual vector quantization [31] for ease of multimodal input and outputs of a unified LLM. In addition, a sequence of slot tokens are trained to be aligned with a sequence of textual inputs using image-text paired data to facilitate the cross-modal understanding and generation in the LLM.

The object-centric visual tokens extracted by the proposed Slot Q-Former are then incorporated into both inputs and outputs of the LLM, and the corresponding Slot-MLLM is fine-tuned from the base LLM using a single next-token prediction objective through multimodal pre-training and multimodal instruction tuning. Experimental results on various vision-language multimodal benchmarks show that the proposed Slot-MLLM with Slot Q-Former performs better than the baseline MLLM trained under the same conditions with existing visual tokenizers. This performance improvement is particularly prominent on object-centric image understanding and generation tasks including text-based image editing. Importantly, to our knowledge, this is the first work demonstrating the effectiveness of slot attention for large-scale multimodal training with LLMs using real-world images.

To summarize, our main contributions are: (1) an object-centric discretized visual tokenizer by Slot Attention for generative MLLMs, Slot Q-Former; (2) an image-text alignment training of Slot Q-Former to ensure that slot tokens are aligned with texts, enabling efficient MLLM training using

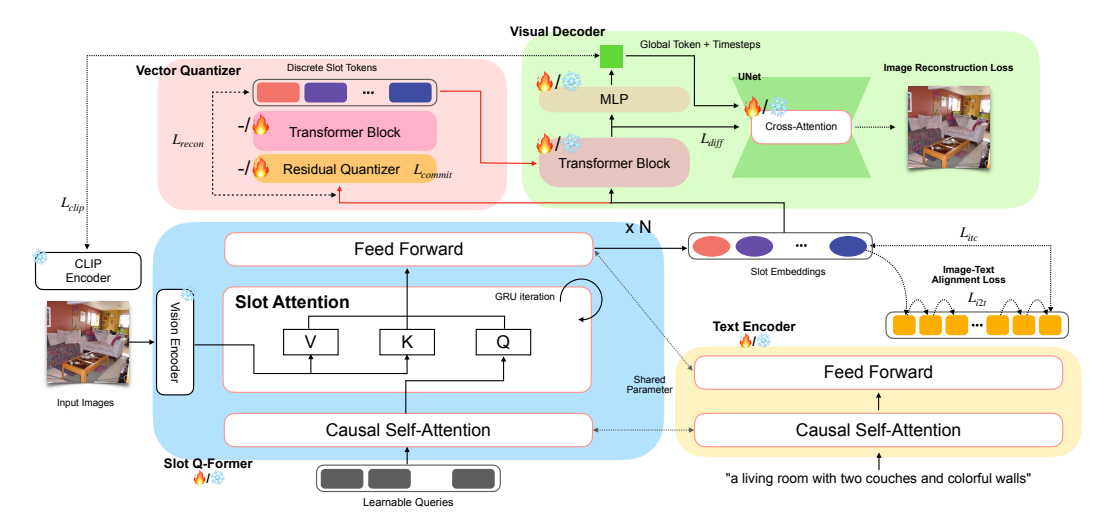


Figure 2: Our tokenizer comprises three main modules: Slot Q-Former, Vector Quantizer, and Visual Decoder. Training occurs in two stages: modules trained in each stage are indicated, and modules exclusive to the second stage—marked in red—include the Vector Quantizer for discrete tokenization.

the unified next-token prediction; and (3) an empirical validation of Slot-MLLM that outperforms baselines due to the use of Slot Q-Former, which is the first-time realization of Slot Attention performed in large-scale LLMs with diverse natural images.

2 Method

The primary goal of this work is to build a generative MLLM that integrates visual and language modalities, ensuring effective object-level control in both image understanding and generation tasks. To achieve this, we propose an object-centric visual tokenizer, named Slot Q-Former, which transforms visual inputs into discrete visual tokens capturing distinct spatial and object-level details of an image. Then, we develop Slot-MLLM, an MLLM that integrates our slot visual tokens and text tokens and performs the multimodal training through a next-token [54, 55] prediction for both image understanding and generation tasks. The overall structure of Slot-MLLM with Slot Q-Former is depicted in Figure 1.

2.1 Object-Centric Slot Q-Former

Motivated by the SEED tokenizer [14], the proposed visual tokenizer consists of three components: Slot Q-Former, Vector Quantizer, and Visual Decoder, to efficiently transform an input image into a sequence of discrete visual tokens to be used as both inputs and outputs of MLLMs. In particular, we integrate Slot Attention [44] into the Q-Former architecture [37], named Slot Q-Former, to ensure that each slot token encapsulates separated object-level information.

Training Slot Q-Former involves two stages. First, Slot Q-Former is trained to extract object-centric information from images. During this stage, the model is trained to reconstruct images using Visual Decoder, simultaneously aligning visual information with text. In the subsequent stage, continuous slot embeddings generated from the first stage is quantized to create discrete tokens suitable for LLM training. Importantly, Slot Q-Former is trained independently from the LLM. This approach enables the encoding of both visual and language data into the same discrete token format, which can be processed as inputs and outputs by MLLMs. The unified token format, in turn, supports flexible integration of various pre-trained LLM backbones.

2.1.1 Architecture

Slot Q-Former. Given an input image $\mathbf{x} \in \mathbb{R}^{H \times W \times C}$, our object-centric Slot Q-Former decomposes the image into a set of N slot visual tokens $S \in \mathbb{R}^{N \times D}$ each corresponding to distinct visual entities. This design aims to facilitate improved comprehension and generation in downstream LLM tasks, as tokens would analogously function as independent language units.

To achieve object-centric representations, we replace a standard cross-attention layer of Q-Former with a slot attention layer that is typically used for object-centric learning. In each slot attention layer, the input image \mathbf{x} is initially processed using a vision encoder f^{Enc} , producing a set of M input features $E = f^{\mathrm{Enc}}(\mathbf{x}) \in \mathbb{R}^{M \times D_{\mathrm{input}}}$. The resulting features E are then grouped into N spatially coherent units, each termed a slot, via an iterative slot refinement process. Here, input learnable slot queries $S \in \mathbb{R}^{N \times D}$ are initialized with Gaussian noise. Competitive attention between queries is then applied, where slots S act as queries, and input features E serve as keys and values. The attention weight $A \in \mathbb{R}^{N \times M}$ is computed by applying a softmax function along the slot dimension, assigning input features to slots: $A = \operatorname{softmax}_N\left(\frac{q(S) \cdot k(E)^T}{\sqrt{D}}\right) \Rightarrow W_{i,j} = \frac{A_{i,j}}{\sum_{n=1}^N A_{n,j}} \Rightarrow U = W \cdot v(E)$.

Here, q,k,v are linear projections that map the learnable slot queries and input features to a common dimension D. $W \in \mathbb{R}^{N \times M}$ represents normalized attention weights across learnable slot queries. The resultant update $U \in \mathbb{R}^{N \times D}$ is subsequently refined through iterative competitive attention employing Gated Recurrent Unit (GRU) [8] structure. The final representation after processing through all slot attention layers within Slot Q-Former is denoted as slot embeddings $S_{emb} = \{s_1, s_2, \dots, s_N\}$.

Additionally, to effectively align visual information with text tokens, Slot Q-Former incorporates a causal self-attention layer following the approach of SEED [14].

Vector Quantizer. Subsequently, slot embeddings S_{emb} generated by the trained Slot Q-Former are converted into discrete tokens, enabling the LLM to interpret them similarly to language tokens. The discrete tokenization allows the LLM to leverage a unified next-token prediction objective efficiently, facilitating the integration of diverse modalities for both inputs and outputs under a single training framework.

Vector Quantizer consists of Residual Vector Quantizer (RVQ) [31] and Transformer block designed to reconstruct slot embeddings from discrete slot tokens. We preliminarily observe that RVQ mitigates the limitations of standard vector quantization used in VQ-VAE [68] and improves the reconstruction quality, motivating its adoption in our method. To further optimize codebook utilization and computational efficiency, we apply dimensionality reduction techniques [53] and use a single shared codebook across all quantization depths. Detailed hyperparameter settings, including the codebook size, are provided in the Appendix.

Visual Decoder. Our Visual Decoder is composed of Transformer decoder block, Multi-Layer Perceptron (MLP), and unCLIP Stable Diffusion (unCLIP-SD) model [57]. Slot embeddings S_{emb} , extracted from Slot Q-Former, pass through a Transformer decoder block f^{Dec} to produce refined embeddings $\hat{S} = f^{Dec}(S_{emb})$. UnCLIP-SD accepts two types of embeddings. Inspired by [25], local embeddings, represented by \hat{S} , condition the UNet [59] of unCLIP-SD via cross-attention layers. And global embeddings, represented by \hat{S}_{global} , are added to timestep embeddings. The global embedding is obtained by an additional MLP head such that $\hat{S}_{global} = \text{MLP}(\hat{S})$.

2.1.2 Continuous Slot Embedding Training

As illustrated in Figure 2, the first stage of tokeinzer training involves learning of Slot Q-Former, Transformer Block, MLP, and Cross-Attention Layer within UNet of unCLIP-SD. Slot Q-Former is initialized with weights from BLIP-2. The first training stage aims to produce continuous slot embeddings S_{emb} and is guided by two primary objectives: image reconstruction and image-text alignment. These two objectives are jointly trained during this stage.

Image Reconstruction Loss. The global token \hat{S}_{global} is trained to be aligned with the CLIP [56] image embedding I using Mean Squared Error (MSE) loss: $\mathcal{L}_{clip} = ||\hat{S}_{global} - I||^2$.

Using both the local condition \hat{S} and global condition \hat{S}_{global} , we train the denoising process of unCLIP-SD in Visual Decoder. Following the standard diffusion model training [19, 58], the UNet model g^{UNet} is trained to predict the noise $\hat{\epsilon}_t$ added to the latent representation z_t at each timestep t: $\hat{\epsilon}_t = g^{\text{UNet}}(z_t, t + \hat{S}_{global}, \hat{S}) \Rightarrow \mathcal{L}_{diff} = ||\hat{\epsilon}_t - \epsilon_t||^2$.

This diffusion-based training approach leverages object-centric slot embeddings, enabling Visual Decoder to accurately reconstruct images while preserving detailed information about individual objects within the scene.

Image-Text Alignment Loss. Despite effective image reconstruction, slot embeddings should be compatible with textual tokens for efficient training with LLMs. To ensure alignment between visual

and textual modalities, we introduce two additional objectives: Image-Text Contrastive Loss (\mathcal{L}_{itc}) and Image-Grounded Text Generation Loss (\mathcal{L}_{i2t}). Inspired by BLIP-2 [37], we share parameters between the causal self-attention layer and feed forward layer in Slot Q-Former and the text encoder, facilitating better textual alignment of slot embeddings.

Specifically, in contrast to BLIP-2 and SEED [14], we maintain causal masking within self-attention when encoding text, preserving token-level causality. The resulting final slot embedding s_N and final text embedding ℓ are used for contrastive learning [50] to further enhance the alignment and causal

which chooding text, preserving token-level causanty. The fortuning final stote inflocting
$$s_N$$
 and final text embedding ℓ are used for contrastive learning [50] to further enhance the alignment and causal structure of slot embeddings: $\mathcal{L}_{itc} = -\log \frac{\exp(s_N^{(i)T}\ell^{(i)}/\tau)}{\sum_{j=1}^B \exp(s_N^{(i)T}\ell^{(j)}/\tau)} - \log \frac{\exp(\ell^{(i)T}s_N^{(i)}/\tau)}{\sum_{j=1}^B \exp(\ell^{(i)T}s_N^{(j)}/\tau)}$,

where B and τ denote the batch size and learnable temperature parameter, respectively. Image-Grounded Text Generation Loss mimics the autoregressive text prediction approach of BLIP-2 by predicting text tokens conditioned on slot tokens: $\mathcal{L}_{i2t} = -\sum_{i} \log P(y_i|s_1, \dots, s_N, y_1, \dots, y_{i-1}),$

where y_i denotes the *i*-th text token. Finally, the first training stage optimizes the weighted sum of four losses: $\mathcal{L}_1 = w_1 \mathcal{L}_{clip} + w_2 \mathcal{L}_{diff} + w_3 \mathcal{L}_{itc} + w_4 \mathcal{L}_{i2t}$.

2.1.3 Discrete Slot Token Training

As depicted in Figure 2, the quantization training stage transforms continuous slot embeddings into discrete slot tokens. During this stage, the weights of Slot Q-Former and Visual Decoder are frozen. Instead, we train only the RVQ and an additional Transformer block to reconstruct the slot embeddings. Similar to standard residual vector quantization methods [31], the training leverages two primary losses: Embedding Reconstruction Loss \mathcal{L}_{recon} and Commitment Loss \mathcal{L}_{commit} , defined as follows: $\mathcal{L}_{recon} = ||S'_{emb} - S_{emb}||_2^2$, $\mathcal{L}_{commit} = \sum_{k=1}^K ||Z - sg[\hat{Z}^{(k)}]||_2^2$.

Here, S_{emb} denotes the original continuous slot embeddings produced by the Slot Q-Former, while S'_{emb} represents their reconstruction after the RVQ module and the additional Transformer block. The RVQ operates for K stages, re-using a single shared codebook. We denote by Z the compressed features from continuous slot embeddings for RVQ, and by $\hat{Z}^{(k)}$ which is the quantized features at depth k. The operator $\operatorname{sg}[\cdot]$ is the stop-gradient function that prevents gradients from flowing into its argument when computing the commitment loss.

Although Visual Decoder is frozen during this stage, the diffusion-based image reconstruction loss, \mathcal{L}_{diff} , \mathcal{L}_{clip} , utilized in the first training stage, are retained and serve as guides for quantization learning. Therefore, the final training loss used in this quantization stage is a weighted sum of four losses: $\mathcal{L}_2 = w_5 \mathcal{L}_{recon} + w_6 \mathcal{L}_{commit} + w_7 \mathcal{L}_{diff} + w_8 \mathcal{L}_{clip}$.

2.2 Slot-MLLM: Multimodal LLM using Slot Visual Tokens

Based on Slot Q-Former, we introduce Slot-MLLM, a generative multimodal LLM. Slot Q-Former discretizes images into object-centric visual tokens, seamlessly integrated with textual tokens in the LLM vocabulary via special tokens (<boi>>, <eoi>>). The depth dimension introduced by RVQ is flattened, enabling standard autoregressive next-token prediction training without altering the LLM's architecture or loss function, while keeping the trained Slot Q-Former frozen during the training of LLM. To improve training efficiency, Low-Rank Adaptation (LoRA) [20] is employed during both the pre-training stage and the instruction tuning stage.

Multimodal Pre-training. In the pre-training stage, we use both image-text paired datasets and interleaved datasets. To avoid unconditional generation, the loss is computed only on the output modality in pair instances and exclusively on the textual parts in interleaved instances. The model is trained under the next-token prediction objective, where a sequence of visual tokens is trained to align with the associated textual inputs.

Multimodal Instruction Tuning. We perform an additional instruction tuning using supervised fine-tuning (SFT) on publicly available multimodal instruction-following datasets. This instruction tuning enhances the model's ability to follow natural language instructions and improves its comprehension and generation capabilities in complex multimodal scenarios. The instruction format "USER: <Instruction> ASSISTANT: <Answer>" is adopted, with the training loss computed exclusively on the <Answer> portion.

Table 1: Image reconstruction performances of visual tokenizers. We compare Slot Q-Former against other diffusion-based visual tokenizers on the COCO Karpathy test set [39]. Metrics include semantic (CLIP-T), perceptual (DreamSIM, LPIPS), and pixel-level (PSNR, SSIM) similarity. Slot Q-Former consistently achieves superior reconstruction quality across most metrics.

Method	CLIP-T ↑	DreamSIM↓	LPIPS↓	PSNR ↑	SSIM↑
LaViT [26]	25.63	0.3185	0.6558	10.76	0.2910
SEED [14]	24.45	0.4132	0.7741	9.51	0.2568
Slot Q-Former	24.95	0.3166	0.5559	12.14	0.2645

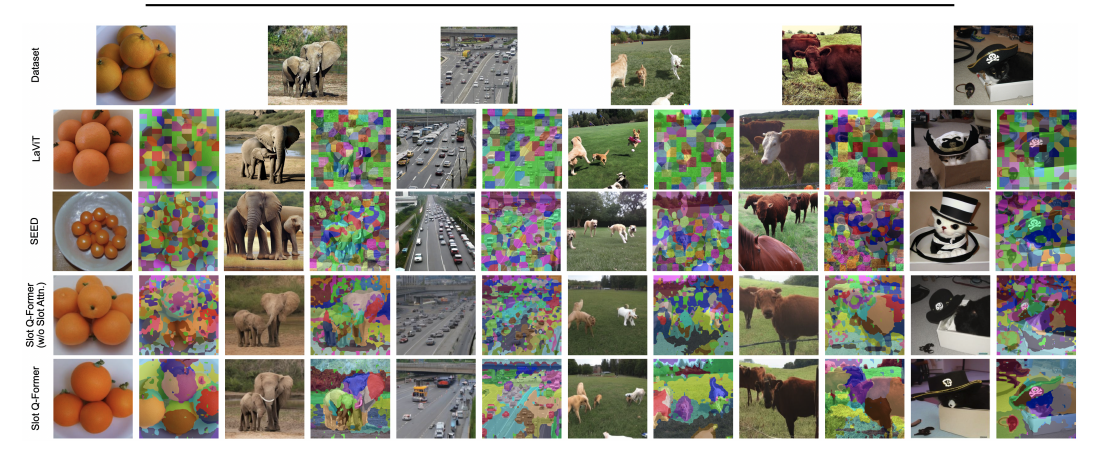


Figure 3: Qualitative results of visual tokenizers. This figure visualizes the reconstructed images generated by various tokenizers, along with the corresponding image regions attended by each token. Slot Q-Former effectively captures object-centric representations by aligning token attention with distinct objects within the image, and can reconstruct images that preserve the original object structures and compositions.

3 Experiments

3.1 Experimental Setup

For Slot Q-Former, we adopt DINOv2 [51] as our vision encoder due to its proficiency in extracting rich local semantic information. The training dataset for Slot Q-Former includes 70 million image-text pairs from CC3M [62], CC12M [6], a subset of LAION-COCO [1], MSCOCO [39], and Unsplash[2]. The first training stage, involving Slot Q-Former and Visual Decoder, is trained on 8 NVIDIA H100 (80GB) GPUs for approximately 48 hours. The second stage, focusing on RVQ, takes about 23 hours using the same GPU resource.

The proposed Slot Q-Former can be universally applied to any pretrained LLM without architectural modifications; in our experiments, we adopt Vicuna-7B [84] as the base LLM. Multimodal pretraining is performed using image-text paired datasets with randomized modality order to support both captioning and generation. We further employ MMC4 [85] as the interleaved dataset. Pretraining is conducted on 8 NVIDIA H100 (80GB) GPUs for approximately 50 hours. Subsequently, multimodal instruction tuning via SFT is performed on diverse task datasets, using the same GPU resource for around 43 hours. The datasets, prompt formats, and other training details are provided in the Appendix.

3.2 Evaluation of Slot Q-Former

The image reconstruction experiments assess the effectiveness of Slot Q-Former in preserving visual details when converting images into discrete tokens, as shown in Table 1. Performance is assessed by measuring semantic similarity to the original text input (CLIP-T [56]), perceptual similarity with human perception (DreamSIM [13], LPIPS [81]), and pixel-level fidelity (PSNR, SSIM [70]) between reconstructed image and ground-truth image. Slot Q-Former is compared with other discrete tokenizers, SEED [14] and LaViT [26], since these visual tokenizers are trained independently of the LLM and employ diffusion-based decoders, closely aligning with the core design of Slot Q-Former.

Table 2: Evaluation on multimodal understanding benchmarks comparing Slot-MLLM against existing MLLMs. To ensure fair comparison, SEED-LLaMA, Slot-MLLM-base, and Slot-MLLM are trained under the same conditions, except for the visual tokenizer. * denotes a performance obtained by our own evaluation using the publicly available checkpoint. For all metrics, higher scores indicate better performance. The best scores among models trained under the same conditions are marked in **bold**. LaViT is not trained with interleaved input prompts, and is thus excluded from benchmarks requiring multi-image inputs.

Method	LLM	COCO Caption	GQA	мме-р	SEED-Bench (Img)	POPE	MM-Vet	MMMU (val)	NaturalBench
MorphTokens SETOKIM	Vicuna-7B LLaMA-2-7B	-	56.8 65.6	1477.7 1537.8	-	- 89.1	45.2	-	-
LaViT	LLaMA-7B	133.9*	46.8	964.5*	35.0*	83.4*	22.6*	29.2*	52.6*
VILA-U	LLaMA-2-7B	90.7*	58.3	1336.2	61.9*	83.9	27.7		63.1*
SEED-LLaMA	Vicuna-7B	122.5*	52.4*	1123.9*	48.6*	78.0*	21.3*	26.8*	57.5
Slot-MLLM-base	Vicuna-7B	119.39	53.8	1128.4	44.7	78.3	17.8	29	59.0
Slot-MLLM	Vicuna-7B	126.8	58.1	1202.6	47.4	79.8	20.6	28	60.5

Table 3: Evaluation on text-to-image and editing benchmarks. * denotes performance obtained by our own evaluation using the publicly available checkpoint. Slot-MLLM outperforms baselines on both localized image editing and compositional image generation tasks. VILA-U is not trained on multimodal prompts for image editing (IT2I); thus, it is not evaluated on editing benchmarks.

Method	Res.	T2I-	T2I-Compbench(↑)		Geneval(↑)	$\textbf{GenAI-Bench}(\uparrow)$		MagicBrush		EVR	
	11051	color	shape	texture	Gene (m)	Basic	Advanced	CLIP-I(↑)	L1(↓)	CLIP-I(↑)	L1(↓)
MorphTokens	-	-	-	-	-	-	-	87.9	7.6	82.6	15.3
SETOKIM	-	-	-	-	-	-	-	89.6	6.3	83.5	14.1
LaViT	1024	0.2730*	0.3191*	0.3988*	0.48*	0.78*	0.62*	78.5*	28.6*	69.1*	30.5*
VILA-U	256	0.5389*	0.4123*	0.5079*	0.42*	0.76*	0.64*	-	-	-	-
SEED-LLaMA	768	0.1741*	0.2033*	0.2361*	0.29*	0.52*	0.49*	77.9*	28.8*	68.6*	31.1*
Slot-MLLM-base	768	0.1512	0.1766	0.2118	0.24	0.46	0.43	77.2	28.2	67.4	30.2
Slot-MLLM	256	0.2756	0.1990	0.2879	0.31	0.58	0.50	82.2	18.6	66.9	20.8

The results show that Slot Q-Former achieves superior performances across multiple metrics. Here, it is noted that LaViT produces much more tokens than Slot Q-Former (avg. 94 vs. 32), which can be beneficial for image reconstruction but makes training MLLMs more challenging.

Qualitative Analysis of Slot Tokens. Figure 3 compares reconstructed images and attention maps qualitatively. Slot Q-Former effectively maintains the original object positions and scene composition in reconstructed images. Furthermore, attention maps demonstrate that Slot Q-Former successfully generates object-centric tokens, distinctly capturing individual objects.

In comparison, LaViT uses a larger number of visual tokens than Slot Q-Former, as shown in its attention map, but struggles to preserve the spatial arrangement of objects, resulting in reconstructed images with shifted object positions. On the other hand, SEED primarily maintains global scene-level semantics, with attention maps dispersed across the entire image rather than focusing on individual objects. Note that when we replace the slot attention with the cross attention (Slot Q-Former w/o Slot Attn), attention maps become dispersed as in SEED, causing object position to shift. This demonstrates the effectiveness of the slot attention in obtaining object-centric tokens.

3.3 Evaluation of Slot-MLLM

3.3.1 Object-Centric Multimodal Understanding

Table 2 shows the comparison between Slot-MLLM and other vision-language MLLMs on various zero-shot multimodal understanding benchmarks, including image captioning and visual question answering (VQA) tasks. Image captioning performance is measured by CIDEr scores [69] on the COCO Karpathy test split [39]. For VQA, we use GQA [24], MME [12], SEED-Bench [35], POPE [38], MM-Vet [78], MMMU [79], and NaturalBench [33], which assess object understanding and logical reasoning capabilities. Notably, GQA focuses on compositional reasoning involving object attributes and relationships derived from Visual Genome scene graphs [30].

Experimental results indicate Slot-MLLM performs better than LaViT [26], SEED-LLaMA [14], and our baseline model (Slot-MLLM-base), which utilizes only MSE loss between CLIP-I embedding and global token \mathcal{L}_{clip} similar to SEED without employing Slot Attention, across most benchmarks. Slot



Figure 4: Qualitative results on image editing tasks. Slot-MLLM effectively modifies specific objects described by text prompts while preserving the overall image composition and context.

Attention effectively segments images into object-centric visual tokens, significantly improving the LLM's ability to comprehend visual scenes, especially in tasks such as GQA requiring understanding of object attributes, spatial relationships, and logical reasoning. These findings highlight the effectiveness of the proposed slot visual tokens in enhancing multimodal understanding. Here, SETOKIM [73] shows better results than Slot-MLLM on some benchmarks. However, SETOKIM employs an ad-hoc clustering and merging for tokenization, differing from our fully end-to-end unsupervised training approach, and moreover conducts approximately 20 times more MLLM training iterations than ours. In addition, SETOKIM jointly trains its tokenizer with the LLM, whereas our method independently trains the tokenizer and the LLM, providing the flexibility in integration with various LLMs. While VILA-U [74] also outperforms Slot-MLLM on several benchmarks, its tokenizer requires a large-scale dataset comprising 700M image-text pairs, which is about 10 times larger than ours, and generates significantly more tokens than Slot Q-Former (256 vs. 32).

3.3.2 Object-Centric Multimodal Generation

Table 3 compares Slot-MLLM to unified MLLMs for understanding and generation on text-to-image generation and image editing benchmarks. T2I-Compbench [21], Geneval [15], and GenAI-Bench [32] evaluate the accuracy and compositional fidelity of generated images in capturing object-level semantics (e.g., color, position, quantity, and texture) described in textual prompts. Additionally, MagicBrush [80] and EVR [67] respectively evaluate the model's capability for localized image editing and more comprehensive, Photoshop-style modification, using metrics such as CLIP similarity (CLIP-I) and pixel-level differences (L1) between generated images and ground-truth images.

Notably, Slot-MLLM consistently outperforms SEED-LLaMA and Slot-MLLM-base across these benchmarks. This demonstrates the effectiveness of object-centric visual tokens, which successfully capture detailed object-level information within each token despite using discrete tokens. Moreover, qualitative examples of image editing presented in Figure 4 clearly illustrate that Slot-MLLM effectively maintains background consistency and handles object-level manipulation capability that other models fail to demonstrate. These results underscore the practical advantage of Slot Q-Former for an unified MLLM, reinforcing its strength in both multimodal generation and image editing tasks. SETOKIM achieves superior editing performance compared to Slot-MLLM due to its difference in training setting and strategy. Also, models using discrete visual tokens similar to Slot-MLLM, such as LaViT and VILA-U, struggle with object-centric editing tasks. Although LaViT and VILA-U employ a larger number of tokens and thus exhibit strong general text-to-image generation performance, LaViT falls short compared to Slot-MLLM in editing tasks, and VILA-U entirely lacks supervised fine-tuning specifically for editing, resulting in poor performance in localized editing scenarios. MorphTokens is difficult to reproduce due to the unavailability of both its code and model checkpoints.

3.4 Ablation Study

To validate the effectiveness of the key components in our proposed methodology, we conduct a comprehensive ablation study. Specifically, we modify Slot Q-Former and the corresponding Slot-MLLM and then evaluate their performances, as shown in Table 4. The detailed configurations and their results are as follows:

Table 4: Ablation results on Slot Q-Former and Slot-MLLM. The table reports reconstruction quality (LPIPS, PSNR), multimodal understanding (GQA, MME-P), and generation performance (Geneval, MagicBrush CLIP-I) when ablating Slot Attention, image reconstruction diffusion loss, and imagetext alignment loss.

Method	Toke	nizer	Under	rstanding	Generation		
	LPIPS(↓)	PSNR(↑)	GQA(↑)	MME-P(↑)	Geneval(↑)	$\textbf{MagicBrush-CLIP-I}(\uparrow)$	
Slot-MLLM	0.5559	12.14	58.1	1202.6	0.31	82.2	
w/o Slot Attention	0.5678	12.21	57.4	1119.0	0.25	80.3	
w/o Slot Attention and Diffusion Loss	0.782	9.42	53.8	1128.4	0.24	77.2	
w/o Image-Text Alignment Loss	0.4222	14.41	52.7	961.6	0.22	81.4	

- (1) w/o Slot Attention: we evaluate the performance impact of slot attention by comparing Slot Q-Former to a baseline model that utilize not the slot attention but the standard cross attention in the Q-Former. Without the slot attention, the results demonstrate significant performance degradation across vision-language tasks that require detailed local comprehension and generation capabilities. As illustrated in Figure 3, the attention maps reveal that tokens without the slot attention fail to distinctly associate with individual objects or specific image regions. Consequently, the slot attention leads the MLLM to enhance overall multimodal task performances.
- (2) w/o Slot Attention and Diffusion Loss (Slot-MLLM-base): we evaluate the effect of diffusion-based image reconstruction loss for the tokenizer training by removing both the slot attention and the diffusion loss. This leads to a significant decline in image reconstruction fidelity, leading to more inferior multimodal understanding and generation performances. The results highlight that diffusion loss specifically supports the preservation of high-quality visual details. Thus, diffusion loss is essential for maintaining fine-grained visual representation, facilitating robust performances in downstream complex multimodal tasks.
- (3) w/o Image-Text Alignment Loss: we remove both the image-text contrastive loss and image-grounded text generation loss from the first training stage of Slot Q-Former. Although the reconstruction performance remains relatively strong, there is a notable decline in the performances of MLLM due to less alignment between slot embeddings and textual information. Therefore, the image-text alignment for the slot visual tokenization is essential for effective integration between visual and textual modalities in the MLLM.

4 Related Works

MLLMs. Recent advances in multimodal large language models (MLLMs), such as [37, 42], primarily focus on multimodal understanding rather than generation. Generative MLLMs, including [9, 14, 26, 29, 52, 66, 74, 75, 77], extend LLMs for image generation. SEED [14] is notable for introducing causal visual tokens using diffusion models, but it captures mainly global semantics, limiting detailed visual understanding.

Visual Tokenizer. Visual tokenizers typically rely on vector quantization methods like VQ-VAE [68] or ViT encoders [10], often producing global or uniformly segmented visual tokens. Recent approaches such as SeTok [73] introduce local semantics but require explicit clustering methods, restricting scalability and flexibility.

Slot Attention. Slot Attention [44] effectively generates unsupervised, object-centric image representations. Previous works like LSD [25] have successfully combined Slot Attention with generative models for reconstruction tasks. While previous works have explored Slot Attention, their performances have not been thoroughly demonstrated at large scale, particularly in integration with LLMs and in-the-wild images. MorphTokens [52] also attempted to include Slot Attention, but clear improvements via Slot Attention have not been well established, and moreover the visual tokens for image generation are separated from those for image understanding.

5 Discussion

Although Slot-MLLM provides competitive multimodal understanding and generation ability, several limitations and potential areas for further improvements remain. First, while our approach utilizes a fixed number of visual tokens, future research could explore dynamically adjusting the number of

visual tokens based on the complexity or content of an input image, potentially enhancing flexibility and efficiency. We apply our proposed Slot Q-Former to various LLM backbones, and include the experimental results with Qwen-2.5-14B [76] in the Appendix as an example. Additionally, extending the current methodology to handle video data represents another promising direction, enabling richer multimodal interactions and temporal reasoning.

6 Conclusion

In this study, we introduce a novel object-centric discretized visual tokenizer, Slot Q-Former, leveraging the slot attention mechanism specifically tailored for generative MLLMs. Our proposed Slot Q-Former effectively preserves local visual details within discrete tokens, maintaining high-level semantics and aligning seamlessly with textual data, thereby enabling efficient multimodal input and output in LLMs. Extensive experiments demonstrate that this Slot-MLLM achieves significant performance improvements over baseline MLLMs on various vision-language benchmarks, particularly excelling in object-centric image understanding and generation tasks, including precise image editing. To our knowledge, this is the first demonstration of successfully scaling Slot Attention to large-scale multimodal training with diverse real-world images.

Acknowledgements

This work was partly supported by Institute of Information & communications Technology Planning & Evaluation (IITP) grant funded by the Korea government(MSIT) (No. RS-2019-II190079, Artificial Intelligence Graduate School Program(Korea University), 15%), the Institute of Information & Communications Technology Planning & Evaluation(IITP)-ITRC(Information Technology Research Center) grant funded by the Korea government(MSIT)(IITP-2025-RS-2024-00436857, 35%), and the National Research Foundation of Korea(NRF) grant funded by the Korea government(MSIT) (No. RS-2024-00353007, 50%).

References

- [1] Laion coco: 600m synthetic captions from laion2b-en. https://github.com/unsplash/datasets.
- [2] Unsplash. https://github.com/unsplash/datasets.
- [3] Manoj Acharya, Kushal Kafle, and Christopher Kanan. Tallyqa: Answering complex counting questions. In *Proceedings of the AAAI conference on artificial intelligence*, volume 33, pages 8076–8084, 2019.
- [4] Jinbin Bai, Wei Chow, Ling Yang, Xiangtai Li, Juncheng Li, Hanwang Zhang, and Shuicheng Yan. Humanedit: A high-quality human-rewarded dataset for instruction-based image editing. *arXiv preprint arXiv:2412.04280*, 2024.
- [5] Tim Brooks, Aleksander Holynski, and Alexei A Efros. Instructpix2pix: Learning to follow image editing instructions. In *Proceedings of the IEEE/CVF conference on computer vision and pattern recognition*, pages 18392–18402, 2023.
- [6] Soravit Changpinyo, Piyush Sharma, Nan Ding, and Radu Soricut. Conceptual 12m: Pushing web-scale image-text pre-training to recognize long-tail visual concepts, 2021.
- [7] Xinlei Chen, Hao Fang, Tsung-Yi Lin, Ramakrishna Vedantam, Saurabh Gupta, Piotr Dollár, and C Lawrence Zitnick. Microsoft coco captions: Data collection and evaluation server. *arXiv* preprint arXiv:1504.00325, 2015.
- [8] Kyunghyun Cho, Bart Van Merriënboer, Caglar Gulcehre, Dzmitry Bahdanau, Fethi Bougares, Holger Schwenk, and Yoshua Bengio. Learning phrase representations using rnn encoderdecoder for statistical machine translation. arXiv preprint arXiv:1406.1078, 2014.
- [9] Runpei Dong, Chunrui Han, Yuang Peng, Zekun Qi, Zheng Ge, Jinrong Yang, Liang Zhao, Jianjian Sun, Hongyu Zhou, Haoran Wei, et al. Dreamllm: Synergistic multimodal comprehension and creation. *arXiv preprint arXiv:2309.11499*, 2023.

- [10] Alexey Dosovitskiy, Lucas Beyer, Alexander Kolesnikov, Dirk Weissenborn, Xiaohua Zhai, Thomas Unterthiner, Mostafa Dehghani, Matthias Minderer, Georg Heigold, Sylvain Gelly, et al. An image is worth 16x16 words: Transformers for image recognition at scale. arXiv preprint arXiv:2010.11929, 2020.
- [11] Patrick Esser, Robin Rombach, and Bjorn Ommer. Taming transformers for high-resolution image synthesis. In *Proceedings of the IEEE/CVF conference on computer vision and pattern recognition*, pages 12873–12883, 2021.
- [12] Chaoyou Fu, Peixian Chen, Yunhang Shen, Yulei Qin, Mengdan Zhang, Xu Lin, Jinrui Yang, Xiawu Zheng, Ke Li, Xing Sun, et al. Mme: A comprehensive evaluation benchmark for multimodal large language models. *arXiv preprint arXiv:2306.13394*, 2023.
- [13] Stephanie Fu, Netanel Tamir, Shobhita Sundaram, Lucy Chai, Richard Zhang, Tali Dekel, and Phillip Isola. Dreamsim: Learning new dimensions of human visual similarity using synthetic data. *arXiv preprint arXiv:2306.09344*, 2023.
- [14] Yuying Ge, Sijie Zhao, Ziyun Zeng, Yixiao Ge, Chen Li, Xintao Wang, and Ying Shan. Making llama see and draw with seed tokenizer. *arXiv preprint arXiv:2310.01218*, 2023.
- [15] Dhruba Ghosh, Hannaneh Hajishirzi, and Ludwig Schmidt. Geneval: An object-focused framework for evaluating text-to-image alignment. *Advances in Neural Information Processing Systems*, 36:52132–52152, 2023.
- [16] Yash Goyal, Tejas Khot, Douglas Summers-Stay, Dhruv Batra, and Devi Parikh. Making the v in vqa matter: Elevating the role of image understanding in visual question answering. In *Proceedings of the IEEE conference on computer vision and pattern recognition*, pages 6904–6913, 2017.
- [17] Danna Gurari, Qing Li, Abigale J Stangl, Anhong Guo, Chi Lin, Kristen Grauman, Jiebo Luo, and Jeffrey P Bigham. Vizwiz grand challenge: Answering visual questions from blind people. In *Proceedings of the IEEE conference on computer vision and pattern recognition*, pages 3608–3617, 2018.
- [18] Guiming Hardy Chen, Shunian Chen, Ruifei Zhang, Junying Chen, Xiangbo Wu, Zhiyi Zhang, Zhihong Chen, Jianquan Li, Xiang Wan, and Benyou Wang. Allava: Harnessing gpt4v-synthesized data for a lite vision-language model. *arXiv e-prints*, pages arXiv–2402, 2024.
- [19] Jonathan Ho, Ajay Jain, and Pieter Abbeel. Denoising diffusion probabilistic models. *Advances in neural information processing systems*, 33:6840–6851, 2020.
- [20] Edward J. Hu, Yelong Shen, Phillip Wallis, Zeyuan Allen-Zhu, Yuanzhi Li, Shean Wang, Lu Wang, and Weizhu Chen. Lora: Low-rank adaptation of large language models, 2021.
- [21] Kaiyi Huang, Kaiyue Sun, Enze Xie, Zhenguo Li, and Xihui Liu. T2i-compbench: A comprehensive benchmark for open-world compositional text-to-image generation. *Advances in Neural Information Processing Systems*, 36:78723–78747, 2023.
- [22] Shih-Cheng Huang, Liyue Shen, Matthew P Lungren, and Serena Yeung. Gloria: A multimodal global-local representation learning framework for label-efficient medical image recognition. In Proceedings of the IEEE/CVF international conference on computer vision, pages 3942–3951, 2021.
- [23] Ting-Hao Huang, Francis Ferraro, Nasrin Mostafazadeh, Ishan Misra, Aishwarya Agrawal, Jacob Devlin, Ross Girshick, Xiaodong He, Pushmeet Kohli, Dhruv Batra, et al. Visual storytelling. In *Proceedings of the 2016 conference of the North American chapter of the association for computational linguistics: Human language technologies*, pages 1233–1239, 2016.
- [24] Drew A Hudson and Christopher D Manning. Gqa: A new dataset for real-world visual reasoning and compositional question answering. In *Proceedings of the IEEE/CVF conference* on computer vision and pattern recognition, pages 6700–6709, 2019.
- [25] Jindong Jiang, Fei Deng, Gautam Singh, and Sungjin Ahn. Object-centric slot diffusion. *arXiv* preprint arXiv:2303.10834, 2023.

- [26] Yang Jin, Kun Xu, Liwei Chen, Chao Liao, Jianchao Tan, Quzhe Huang, Bin Chen, Chenyi Lei, An Liu, Chengru Song, et al. Unified language-vision pretraining in llm with dynamic discrete visual tokenization. *arXiv* preprint arXiv:2309.04669, 2023.
- [27] Justin Johnson, Bharath Hariharan, Laurens Van Der Maaten, Li Fei-Fei, C Lawrence Zitnick, and Ross Girshick. Clevr: A diagnostic dataset for compositional language and elementary visual reasoning. In *Proceedings of the IEEE conference on computer vision and pattern recognition*, pages 2901–2910, 2017.
- [28] Kushal Kafle, Brian Price, Scott Cohen, and Christopher Kanan. Dvqa: Understanding data visualizations via question answering. In *Proceedings of the IEEE conference on computer vision and pattern recognition*, pages 5648–5656, 2018.
- [29] Jing Yu Koh, Daniel Fried, and Ruslan Salakhutdinov. Generating images with multimodal language models, 2023.
- [30] Ranjay Krishna, Yuke Zhu, Oliver Groth, Justin Johnson, Kenji Hata, Joshua Kravitz, Stephanie Chen, Yannis Kalantidis, Li-Jia Li, David A Shamma, et al. Visual genome: Connecting language and vision using crowdsourced dense image annotations. *International journal of computer vision*, 123:32–73, 2017.
- [31] Doyup Lee, Chiheon Kim, Saehoon Kim, Minsu Cho, and Wook-Shin Han. Autoregressive image generation using residual quantization. In *Proceedings of the IEEE/CVF Conference on Computer Vision and Pattern Recognition*, pages 11523–11532, 2022.
- [32] Baiqi Li, Zhiqiu Lin, Deepak Pathak, Jiayao Emily Li, Xide Xia, Graham Neubig, Pengchuan Zhang, and Deva Ramanan. Genai-bench: A holistic benchmark for compositional text-to-visual generation. In *Synthetic Data for Computer Vision Workshop@ CVPR 2024*, 2024.
- [33] Baiqi Li, Zhiqiu Lin, Wenxuan Peng, Jean de Dieu Nyandwi, Daniel Jiang, Zixian Ma, Simran Khanuja, Ranjay Krishna, Graham Neubig, and Deva Ramanan. Naturalbench: Evaluating vision-language models on natural adversarial samples. arXiv preprint arXiv:2410.14669, 2024.
- [34] Bo Li, Yuanhan Zhang, Liangyu Chen, Jinghao Wang, Fanyi Pu, Jingkang Yang, Chunyuan Li, and Ziwei Liu. Mimic-it: Multi-modal in-context instruction tuning. arXiv preprint arXiv:2306.05425, 2023.
- [35] Bohao Li, Yuying Ge, Yixiao Ge, Guangzhi Wang, Rui Wang, Ruimao Zhang, and Ying Shan. Seed-bench: Benchmarking multimodal large language models. In *Proceedings of the IEEE/CVF Conference on Computer Vision and Pattern Recognition*, pages 13299–13308, 2024.
- [36] Junnan Li, Dongxu Li, Caiming Xiong, and Steven Hoi. Blip: Bootstrapping language-image pre-training for unified vision-language understanding and generation. In *International conference on machine learning*, pages 12888–12900. PMLR, 2022.
- [37] Junnan Li, Dongxu Li, Silvio Savarese, and Steven Hoi. Blip-2: Bootstrapping language-image pre-training with frozen image encoders and large language models. In *International conference on machine learning*, pages 19730–19742. PMLR, 2023.
- [38] Yifan Li, Yifan Du, Kun Zhou, Jinpeng Wang, Wayne Xin Zhao, and Ji-Rong Wen. Evaluating object hallucination in large vision-language models. *arXiv preprint arXiv:2305.10355*, 2023.
- [39] Tsung-Yi Lin, Michael Maire, Serge Belongie, Lubomir Bourdev, Ross Girshick, James Hays, Pietro Perona, Deva Ramanan, C. Lawrence Zitnick, and Piotr Dollár. Microsoft coco: Common objects in context, 2015.
- [40] Zhiqiu Lin, Deepak Pathak, Baiqi Li, Jiayao Li, Xide Xia, Graham Neubig, Pengchuan Zhang, and Deva Ramanan. Evaluating text-to-visual generation with image-to-text generation. In *European Conference on Computer Vision*, pages 366–384. Springer, 2024.
- [41] Fangyu Liu, Guy Emerson, and Nigel Collier. Visual spatial reasoning. *Transactions of the Association for Computational Linguistics*, 11:635–651, 2023.
- [42] Haotian Liu, Chunyuan Li, Qingyang Wu, and Yong Jae Lee. Visual instruction tuning, 2023.

- [43] Haotian Liu, Chunyuan Li, Yuheng Li, Bo Li, Yuanhan Zhang, Sheng Shen, and Yong Jae Lee. Llavanext: Improved reasoning, ocr, and world knowledge, 2024.
- [44] Francesco Locatello, Dirk Weissenborn, Thomas Unterthiner, Aravindh Mahendran, Georg Heigold, Jakob Uszkoreit, Alexey Dosovitskiy, and Thomas Kipf. Object-centric learning with slot attention. *Advances in neural information processing systems*, 33:11525–11538, 2020.
- [45] Pan Lu, Liang Qiu, Jiaqi Chen, Tony Xia, Yizhou Zhao, Wei Zhang, Zhou Yu, Xiaodan Liang, and Song-Chun Zhu. Iconqa: A new benchmark for abstract diagram understanding and visual language reasoning. *arXiv preprint arXiv:2110.13214*, 2021.
- [46] Kenneth Marino, Mohammad Rastegari, Ali Farhadi, and Roozbeh Mottaghi. Ok-vqa: A visual question answering benchmark requiring external knowledge. In *Proceedings of the IEEE/cvf conference on computer vision and pattern recognition*, pages 3195–3204, 2019.
- [47] Ahmed Masry, Xuan Long Do, Jia Qing Tan, Shafiq Joty, and Enamul Hoque. Chartqa: A benchmark for question answering about charts with visual and logical reasoning. In *Findings of the Association for Computational Linguistics: ACL 2022*, pages 2263–2279, 2022.
- [48] Minesh Mathew, Dimosthenis Karatzas, and CV Jawahar. Docvqa: A dataset for vqa on document images. In *Proceedings of the IEEE/CVF winter conference on applications of computer vision*, pages 2200–2209, 2021.
- [49] Anand Mishra, Shashank Shekhar, Ajeet Kumar Singh, and Anirban Chakraborty. Ocr-vqa: Visual question answering by reading text in images. In *2019 international conference on document analysis and recognition (ICDAR)*, pages 947–952. IEEE, 2019.
- [50] Aaron van den Oord, Yazhe Li, and Oriol Vinyals. Representation learning with contrastive predictive coding. *arXiv* preprint arXiv:1807.03748, 2018.
- [51] Maxime Oquab, Timothée Darcet, Théo Moutakanni, Huy Vo, Marc Szafraniec, Vasil Khalidov, Pierre Fernandez, Daniel Haziza, Francisco Massa, Alaaeldin El-Nouby, et al. Dinov2: Learning robust visual features without supervision. *arXiv preprint arXiv:2304.07193*, 2023.
- [52] Kaihang Pan, Siliang Tang, Juncheng Li, Zhaoyu Fan, Wei Chow, Shuicheng Yan, Tat-Seng Chua, Yueting Zhuang, and Hanwang Zhang. Auto-encoding morph-tokens for multimodal llm. *arXiv* preprint arXiv:2405.01926, 2024.
- [53] Zhiliang Peng, Li Dong, Hangbo Bao, Qixiang Ye, and Furu Wei. BEiT v2: Masked image modeling with vector-quantized visual tokenizers. 2022.
- [54] Alec Radford, Karthik Narasimhan, Tim Salimans, Ilya Sutskever, et al. Improving language understanding by generative pre-training. 2018.
- [55] Alec Radford, Jeffrey Wu, Rewon Child, David Luan, Dario Amodei, Ilya Sutskever, et al. Language models are unsupervised multitask learners. *OpenAI blog*, 1(8):9, 2019.
- [56] Alec Radford, Jong Wook Kim, Chris Hallacy, Aditya Ramesh, Gabriel Goh, Sandhini Agarwal, Girish Sastry, Amanda Askell, Pamela Mishkin, Jack Clark, Gretchen Krueger, and Ilya Sutskever. Learning transferable visual models from natural language supervision, 2021.
- [57] Aditya Ramesh, Prafulla Dhariwal, Alex Nichol, Casey Chu, and Mark Chen. Hierarchical text-conditional image generation with clip latents. *arXiv preprint arXiv:2204.06125*, 1(2):3, 2022.
- [58] Robin Rombach, Andreas Blattmann, Dominik Lorenz, Patrick Esser, and Björn Ommer. High-resolution image synthesis with latent diffusion models. In *Proceedings of the IEEE/CVF conference on computer vision and pattern recognition*, pages 10684–10695, 2022.
- [59] Olaf Ronneberger, Philipp Fischer, and Thomas Brox. U-net: Convolutional networks for biomedical image segmentation. In *Medical image computing and computer-assisted intervention–MICCAI 2015: 18th international conference, Munich, Germany, October 5-9, 2015, proceedings, part III 18*, pages 234–241. Springer, 2015.

- [60] Christoph Schuhmann, Romain Beaumont, Richard Vencu, Cade Gordon, Ross Wightman, Mehdi Cherti, Theo Coombes, Aarush Katta, Clayton Mullis, Mitchell Wortsman, et al. Laion-5b: An open large-scale dataset for training next generation image-text models. Advances in neural information processing systems, 35:25278–25294, 2022.
- [61] Dustin Schwenk, Apoorv Khandelwal, Christopher Clark, Kenneth Marino, and Roozbeh Mottaghi. A-okvqa: A benchmark for visual question answering using world knowledge. In *European conference on computer vision*, pages 146–162. Springer, 2022.
- [62] Piyush Sharma, Nan Ding, Sebastian Goodman, and Radu Soricut. Conceptual captions: A cleaned, hypernymed, image alt-text dataset for automatic image captioning. In *Proceedings of the 56th Annual Meeting of the Association for Computational Linguistics (Volume 1: Long Papers)*, pages 2556–2565, 2018.
- [63] Oleksii Sidorov, Ronghang Hu, Marcus Rohrbach, and Amanpreet Singh. Textcaps: a dataset for image captioning with reading comprehension. In *Computer Vision–ECCV 2020: 16th European Conference, Glasgow, UK, August 23–28, 2020, Proceedings, Part II 16*, pages 742–758. Springer, 2020.
- [64] Amanpreet Singh, Vivek Natarajan, Meet Shah, Yu Jiang, Xinlei Chen, Dhruv Batra, Devi Parikh, and Marcus Rohrbach. Towards vqa models that can read. In *Proceedings of the IEEE/CVF conference on computer vision and pattern recognition*, pages 8317–8326, 2019.
- [65] Keqiang Sun, Junting Pan, Yuying Ge, Hao Li, Haodong Duan, Xiaoshi Wu, Renrui Zhang, Aojun Zhou, Zipeng Qin, Yi Wang, et al. Journeydb: A benchmark for generative image understanding. *Advances in neural information processing systems*, 36:49659–49678, 2023.
- [66] Quan Sun, Qiying Yu, Yufeng Cui, Fan Zhang, Xiaosong Zhang, Yueze Wang, Hongcheng Gao, Jingjing Liu, Tiejun Huang, and Xinlong Wang. Emu: Generative pretraining in multimodality, 2024.
- [67] Hao Tan, Franck Dernoncourt, Zhe Lin, Trung Bui, and Mohit Bansal. Expressing visual relationships via language. *arXiv preprint arXiv:1906.07689*, 2019.
- [68] Aaron van den Oord, Oriol Vinyals, and Koray Kavukcuoglu. Neural discrete representation learning, 2018.
- [69] Ramakrishna Vedantam, C. Lawrence Zitnick, and Devi Parikh. Cider: Consensus-based image description evaluation. 2015 IEEE Conference on Computer Vision and Pattern Recognition (CVPR), pages 4566-4575, 2014. URL https://api.semanticscholar.org/CorpusID: 9026666.
- [70] Zhou Wang, A.C. Bovik, H.R. Sheikh, and E.P. Simoncelli. Image quality assessment: from error visibility to structural similarity. *IEEE Transactions on Image Processing*, 13(4):600–612, 2004. doi: 10.1109/TIP.2003.819861.
- [71] Zijie J Wang, Evan Montoya, David Munechika, Haoyang Yang, Benjamin Hoover, and Duen Horng Chau. Diffusiondb: A large-scale prompt gallery dataset for text-to-image generative models. *arXiv preprint arXiv:2210.14896*, 2022.
- [72] Cong Wei, Zheyang Xiong, Weiming Ren, Xeron Du, Ge Zhang, and Wenhu Chen. Omniedit: Building image editing generalist models through specialist supervision. In *The Thirteenth International Conference on Learning Representations*, 2024.
- [73] Shengqiong Wu, Hao Fei, Xiangtai Li, Jiayi Ji, Hanwang Zhang, Tat-Seng Chua, and Shuicheng Yan. Towards semantic equivalence of tokenization in multimodal llm. *arXiv preprint arXiv:2406.05127*, 2024.
- [74] Yecheng Wu, Zhuoyang Zhang, Junyu Chen, Haotian Tang, Dacheng Li, Yunhao Fang, Ligeng Zhu, Enze Xie, Hongxu Yin, Li Yi, et al. Vila-u: a unified foundation model integrating visual understanding and generation. *arXiv preprint arXiv:2409.04429*, 2024.
- [75] Rongchang Xie, Chen Du, Ping Song, and Chang Liu. Muse-vl: Modeling unified vlm through semantic discrete encoding. *arXiv preprint arXiv:2411.17762*, 2024.

- [76] An Yang, Baosong Yang, Beichen Zhang, Binyuan Hui, Bo Zheng, Bowen Yu, Chengyuan Li, Dayiheng Liu, Fei Huang, Haoran Wei, et al. Qwen2. 5 technical report. *arXiv preprint arXiv:2412.15115*, 2024.
- [77] Lijun Yu, Yong Cheng, Kihyuk Sohn, José Lezama, Han Zhang, Huiwen Chang, Alexander G. Hauptmann, Ming-Hsuan Yang, Yuan Hao, Irfan Essa, and Lu Jiang. Magvit: Masked generative video transformer, 2023.
- [78] Weihao Yu, Zhengyuan Yang, Linjie Li, Jianfeng Wang, Kevin Lin, Zicheng Liu, Xinchao Wang, and Lijuan Wang. Mm-vet: Evaluating large multimodal models for integrated capabilities. arXiv preprint arXiv:2308.02490, 2023.
- [79] Xiang Yue, Yuansheng Ni, Kai Zhang, Tianyu Zheng, Ruoqi Liu, Ge Zhang, Samuel Stevens, Dongfu Jiang, Weiming Ren, Yuxuan Sun, et al. Mmmu: A massive multi-discipline multimodal understanding and reasoning benchmark for expert agi. In *Proceedings of the IEEE/CVF Conference on Computer Vision and Pattern Recognition*, pages 9556–9567, 2024.
- [80] Kai Zhang, Lingbo Mo, Wenhu Chen, Huan Sun, and Yu Su. Magicbrush: A manually annotated dataset for instruction-guided image editing. Advances in Neural Information Processing Systems, 36:31428–31449, 2023.
- [81] Richard Zhang, Phillip Isola, Alexei A Efros, Eli Shechtman, and Oliver Wang. The unreasonable effectiveness of deep features as a perceptual metric. In *Proceedings of the IEEE conference on computer vision and pattern recognition*, pages 586–595, 2018.
- [82] Yanzhe Zhang, Ruiyi Zhang, Jiuxiang Gu, Yufan Zhou, Nedim Lipka, Diyi Yang, and Tong Sun. Llavar: Enhanced visual instruction tuning for text-rich image understanding. *arXiv preprint arXiv:2306.17107*, 2023.
- [83] Bo Zhao, Boya Wu, Muyang He, and Tiejun Huang. Svit: Scaling up visual instruction tuning. arXiv preprint arXiv:2307.04087, 2023.
- [84] Lianmin Zheng, Wei-Lin Chiang, Ying Sheng, Siyuan Zhuang, Zhanghao Wu, Yonghao Zhuang, Zi Lin, Zhuohan Li, Dacheng Li, Eric Xing, et al. Judging llm-as-a-judge with mt-bench and chatbot arena. *Advances in Neural Information Processing Systems*, 36:46595–46623, 2023.
- [85] Wanrong Zhu, Jack Hessel, Anas Awadalla, Samir Yitzhak Gadre, Jesse Dodge, Alex Fang, Youngjae Yu, Ludwig Schmidt, William Yang Wang, and Yejin Choi. Multimodal c4: An open, billion-scale corpus of images interleaved with text, 2023.

Table 5: Summary of Slot Q-Former Training Settings

Configuration	Continuous Slot Embedding Training	Discrete Slot Token Training						
Number of Slots (N)	32							
Slot Dimension (D)	768							
GRU Iteration	3							
Vision Encoder	DINOv2-Large							
Input Image Shape	448 x 448							
Codebook Size	-	8192						
Codebook Dimension	-	32						
Quantization Depth (K)	-	4						
Loss Weight	$w_1: 0.5, w_2: 1, w_3: 0.5, w_4: 0.5$	$w_5: 1, w_6: 1, w_7: 0.1, w_8: 0.1$						
Optimizer	AdamW							
Optimizer Hyperparameters	$\beta_1:0.9,\beta_2:0.999$	$0, \epsilon$: 1e-8						
Weight Decay	0.01							
Max Learning Rate	1e-4							
Learning Rate Scheduler	Linear Warmup, Cosir	ne Annealing						
Warm-up Steps	500							
Local Batch Size	128							
GPU	$8 \times H100 \ 80$	GB						
Training Data	CC15M, LAION-COCO, M	SCOCO, Unsplash						
Data Balance	15:24:1:	4						
Total Training Data	70M	50M						
Mixed Precision	fp16							

A Experiment Setting

A.1 Slot Q-Former

One of the challenges encountered during the first training stage of Slot Q-Former is identifying the optimal balance between losses. To investigate this, we conduct experiments by fixing the weight of the Image Reconstruction Loss, w_1 to 0.5 and w_2 to 1, while varying the weight of the Image-Text Alignment Loss weights, w_3 and w_4 , across values of 0.1, 0.3, 0.5, and 1.0. When the Image-Text Alignment ratio is too high (e.g., 1.0), the image reconstruction performance of the tokenizer degrades significantly, negatively impacting the quality of results produced by Slot-MLLM. Conversely, when the ratio is too low (e.g., 0.1), the tokenizer shows strong reconstruction performance, but Slot-MLLM struggles to predict visual tokens effectively. While a ratio of 0.5 leads to slightly worse tokenizer reconstruction performance compared to 0.3, it ultimately results in better downstream performance for Slot-MLLM, and thus is selected as our final weight balance.

Additionally, we investigate the inclusion of image reconstruction losses (w_7, w_8) during the second training stage. While the reconstruction performance improvement achieved by including these losses is relatively modest, it nonetheless results in a measurable increase in reconstruction quality. Given this improvement, we opt to include these losses in our final training configuration. This optimal weight configuration is summarized in Table 5.

For training data, we use the image-text pair datasets from Slot-MLLM multimodal pre-training stage listed in Table 7, excluding MMC4 [85] which is an interleaved dataset.

A.2 Slot-MLLM

Multimodal Pre-training. We present the multimodal pre-training configurations of Slot-MLLM in Table 6. Detailed descriptions of the training datasets are provided in Table 7.

Multimodal Instruction Tuning. We outline the multimodal instruction tuning configurations of Slot-MLLM in Table 6. Additionally, the datasets and corresponding prompts used for instruction tuning are described as follows:

Table 6: Summary of Slot-MLLM multimodal pre-training and instruction tuning settings. Datasets and their associated local batch size and data ratios used for instruction tuning are omitted due to the large number of datasets.

Configuration	Multimodal Pre-training	Multimodal Instruction Tuning					
LoRA Rank	64	32					
Optimizer	Ada	nmW					
Optimizer Hyperparameters	$\beta_1: 0.9, \beta_2: 0.98, \epsilon: 1e-6$	$\beta_1: 0.9, \beta_2: 0.95, \epsilon: \text{le-5}$					
Weight Decay	0.	05					
Max Learning Rate	3e-4	1e-4					
Learning Rate Scheduler	Linear Warmup, Cosine Annealing						
Total Training Steps	50K	50K					
Warm-up Ratio	0.03	0.05					
Accumulation Step	4	1					
Training Data	(CC15M, MSCOCO, Unsplash), LAION-COCO, MMC4	-					
Local Batch Size per Dataset	20, 20, 5	-					
Data Balance	6:56:38	-					
GPU	$8 \times H10$	00 80GB					
Mixed Precision	bi	f16					

Table 7: Description of datasets used for Slot-MLLM multimodal pre-training.

Dataset Name	Dataset Description
CC3M [62], CC12M [6]	Image-text pair datasets of 3M and 12M sizes, respectively.
LAION-COCO [1]	A 600M-sized image-text pair dataset created by BLIP, from which the top 24M pairs were filtered based on image-caption similarity.
MSCOCO [39]	A 0.5M-sized image-text pair dataset written by humans.
Unsplash [2]	A 4.8M-sized high-quality image-text pair dataset sourced from Unsplash.
MMC4 [85]	A 5.5M-sized image-text interleaved dataset. We use mmc4-core-ff split, and randomly shuffle the order of images and their corresponding text.

- (1) Text-to-Image Generation (T2I): We utilize single-turn datasets, including JourneyDB [65], DiffusionDB [71], and LAION-Aesthetics—a high-quality subset of LAION-5B [60]—as well as the multi-turn dataset VIST [23]. The prompt template is formatted as follows: "USER: {caption}\n ASSISTANT: {image}". The image generation instruction is randomly sampled from a predefined set, such as "Please generate an image", "Can you make an image of", and "Show me a photo of", and then concatenated with the caption.
- (2) Image Editing: We utilize MagicBrush [80], Instructpix2pix [5], HumanEdit [4], and OmniEdit [72], focusing exclusively on single-turn scenarios. Specifically, for OmniEdit, we employ long editing instructions. The prompt template is structured as follows: "USER: {image1} {instruction}\n ASSISTANT: {image2}"
- (3) Image Captioning: We employ COCO Caption [7], TextCaps [63], and VSR [41], adopting the prompt format from SEED-LLaMA [14]: "USER: {image} Please provide an accurate and concise description of the given image.\n ASSISTANT: {caption}"
- (4) Image QA: We leverage various visual question answering (VQA) datasets, including VQAv2 [16], GQA [24], OKVQA [46], A-OKVQA [61], VizWiz [17], TextVQA [64], OCRVQA [49], ChartQA [47], DocVQA [48], DVQA [28], IconQA [45], SVIT [83], and counting-specific datasets such as CLEVR [27] and TallyQA [3]. The prompt template, based on SEED-LLaMA, is formatted as follows: "USER: {image} {question} Please provide an accurate answer consisting of only one word or phrase.\n ASSISTANT: {answer}".

Table 8: Impact of randomly replacing visual tokens on image reconstruction and multimodal understanding performance across Slot Q-Former variants. Performance metrics after token replacement are indicated with the prefix 'Drop' (e.g., Drop LPIPS, Drop GQA), and the values in parentheses denote the changes in performance.

Method		Toker		Understanding				
	$LPIPS(\downarrow)$	Drop LPIPS	PSNR(↑)	Drop PSNR	GQA(↑)	Drop GQA	MME-P(↑)	Drop MME-P
Slot-MLLM	0.5559	0.6789 (+22.1%)	12.14	9.9 (-18.5%)	58.1	49.8 (-14.3%)	1202.6	946.5 (-21.3%)
w/o Slot Attention w/o Slot Attention and Diffusion Loss	0.5678 0.782	0.6819 (+20.1%) 0.8055 (+3.0%)	12.21 9.42	10.35 (-15.23%) 9.09 (-3.5%)	57.4 53.8	50.9 (-11.4%) 49.2 (-8.5%)	1119.0 1128.4	996.2 (-11.0%) 1014.4 (-10.1%)

- (5) Image Conversation: We utilize datasets such as LLaVA-Instruct [42], LLaVA-NeXT-Data [43], SVIT, LLaVAR [82], and ALLaVA [18] to handle multi-turn conversational scenarios involving images. The prompt template is structured as follows: "USER: {image} {question}\n ASSISTANT: {answer}\n..."
- (6) Multi-Image Understanding: We leverage CGD [34] for multi-image comprehension tasks. The prompt template is formatted as follows: "USER: This is the first image. {image1} This is the second image. {image2} {question}\n ASSISTANT: {answer}". The positions of the descriptive phrases ("This is the first image.", "This is the second image.") relative to their corresponding images are randomly varied, appearing either before or after the images, to enhance the robustness of the model.

Evaluation Setup. For evaluating the multimodal comprehension and image generation ability of Slot-MLLM, we use the following benchmarks and prompts across different tasks: In Image Captioning, the evaluation is conducted on the COCO Karpathy test split [39], utilizing the same prompt as that used in instruction tuning. The widely-used CIDEr score [69] is employed as the evaluation metric. For VQA, we adopt a comprehensive set of benchmarks including GQA [24], MME [12], SEED-Bench [35], POPE [38], MM-Vet [78], MMMU [79], and NaturalBench [33]. We utilize the same prompt as that used in instruction tuning. When evaluating SEED-Bench, we follow the official guidelines: for each choice within a question, we calculate the likelihood of the model generating the corresponding choice given the question, and select the choice with the highest likelihood as the model's prediction. Note that our SEED-Bench evaluation is conducted exclusively using the image modality. For the remaining benchmarks, we conduct evaluation by directly generating answers, following their respective official evaluation protocols. Specifically, for MME, we measure only Perception abilities, and for POPE, performance is reported as the average F1 score across three evaluation scenarios: adversarial, popular, and random.

For the T2I task, T2I-Compbench [21], Geneval [15], and GenAI-Bench [32] are used with prompts formatted as "USER: caption Please generate an image.\n ASSISTANT:". T2I-CompBench evaluates compositional image generation performance. Among its eight subcategories, we report the scores for color, shape, and texture. These results are evaluated using BLIP-VQA [36], as specified by the benchmark's official evaluation criteria. GenEval assesses object-focused image generation capabilities through various compositional reasoning tasks. It employs object detection and color classification to verify fine-grained object properties during evaluation. GenAI-Bench evaluates compositional text-to-image generation performance using VQAScore [40], a metric measuring how well generated images align with textual prompts via a VQA model. Lastly, in the image editing task, evaluation datasets include MagicBrush [80] and EVR [67], with metrics such as CLIP similarity (CLIP-I) and pixel-level differences (L1) between generated images and ground-truth images. The prompt used is the same as that in instruction tuning.

B Slot Q-Former Analysis

B.1 Token Analysis

To verify whether each visual token generated by Slot Q-Former effectively encodes distinct and detailed image information, we conduct an experiment in which some visual tokens are replaced with alternative discrete tokens. Specifically, among the 32 discrete visual tokens, we randomly select 50% and replace them with random discrete tokens sampled from the entire codebook range (indices 0–8191). We then evaluate both the reconstruction performance based on these altered discrete visual tokens and their corresponding multimodal understanding performance. If each token distinctly represents different regions or objects within an image, replacing specific tokens would lead to a

Table 9: Ablation results comparing Slot Q-Former, Slot Q-Former with object-level ITC, and Slot Q-Former without image-text alignment loss, along with their corresponding MLLM performance. While employing object-level ITC improves image reconstruction quality, this does not translate into meaningful improvements in downstream MLLM performance.

Method	Tokenizer		Understanding		Generation		
	LPIPS(↓)	PSNR(↑)	GQA(↑)	MME-P(↑)	Geneval(↑)	MagicBrush-CLIP-I(↑)	
Slot-MLLM	0.5559	12.14	58.1	1202.6	0.31	82.2	
w/ Object-Level Image-Text Contrastive Loss	0.5338	12.33	56.8	1199.1	0.31	81.1	
w/o Image-Text Alignment Loss	0.4222	14.41	52.7	961.6	0.22	81.4	

significant loss of information related to the regions encoded by those tokens. Therefore, a substantial change in performance after token replacement would indicate that individual tokens distinctly capture individual objects. Conversely, a minor performance change would imply overlapping or redundant visual information among tokens.

As shown in Table 8, visual tokens generated by the tokenizer without both slot attention and diffusion loss exhibit only slight performance changes upon token replacement. Consequently, this indicates that the tokenizer fails to effectively encode distinct visual details, as each token primarily represents the overall conceptual content of the image rather than specific objects. Similarly, the visual tokenizer without slot attention alone also shows relatively minor performance changes compared to Slot Q-Former. In contrast, visual tokens generated by our proposed Slot Q-Former exhibit the largest performance changes upon replacement, clearly indicating that each token effectively captures distinct and detailed visual information. This finding can also be visually confirmed in Figure 3.

B.2 Object-Level Image-Text Contrastive Loss

Among the Image-Text Alignment Losses described in Section 2.1.2, the Image-Text Contrastive Loss \mathcal{L}_{itc} is trained using the contrastive loss [50] between the final text token and the final image token. However, since this method relies solely on global information from tokens, we explore an improved approach by adopting the localized representation learning method introduced by GLoRIA [22].

Specifically, we define a localized feature matching function utilizing attention weights between each local image feature and each word-level text feature, and apply a local contrastive loss based on this function. This method aims to maximize the posterior probability between the attention-weighted local image representations and corresponding word-level representations.

However, despite this theoretical advantage, our experimental results do not demonstrate performance improvements with this local contrastive loss. We hypothesize that the imbalance among different losses adversely affects tokenizer performance. Although these results are inconclusive, we report them as they may inform future research directions. Results are detailed in Figure 5 and Table 9. In some cases, Slot Q-Former appears to capture finer details from the scene, leading to improved reconstruction quality; however, this does not translate into noticeable improvements in downstream LLM performance.

B.3 Effect of Image-Text Alignment Loss in Slot Q-Former

An important aspect during the training of Slot Q-Former is finding an appropriate balance between the Image-Text Alignment Loss and the Image Reconstruction Loss. As demonstrated in the ablation section 3.4 and Table 9, removing the Image-Text Alignment Loss improves reconstruction performance at the tokenizer level but leads to decreased downstream MLLM performance in understanding and generation tasks.

Figure 5 illustrates the difference in attention maps produced by Slot Q-Former, with and without the Image-Text Alignment Loss. While it appears that Slot Q-Former trained with the Image-Text Alignment Loss produces more object-centric slot attention, this observation is limited to a few case studies and thus requires further validation.

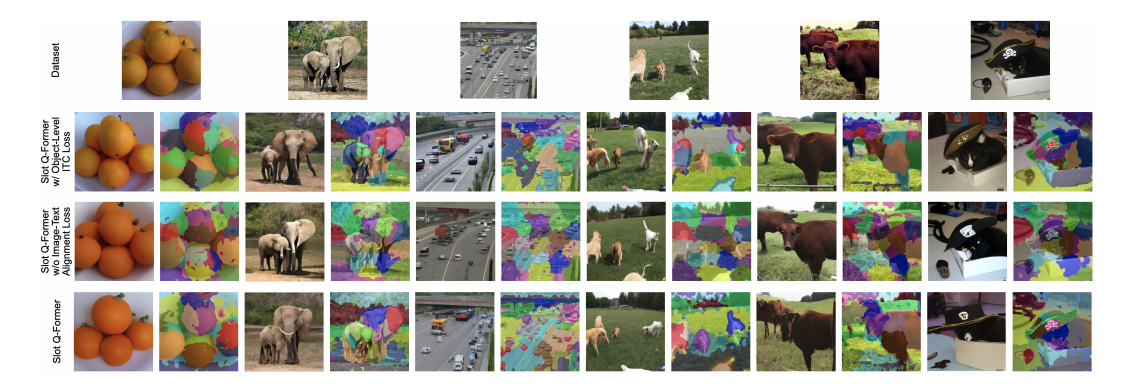


Figure 5: Qualitative results for variations of Slot Q-Former. When using the object-level image-text contrastive loss, multiple slot tokens are sometimes assigned to a single object. In contrast, models trained without the image-text alignment loss exhibit better image reconstruction quality but produce attention maps that are less object-centric. These observations require further validation.

Table 10: Ablation results comparing Slot Q-Former and VQ-GAN Tokenizer. Although the tokenizer reconstruction quality of VQ-GAN is better, it results in poorer downstream performance in the MLLM multimodal understanding tasks. VQ-GAN-MLLM hardly performs multimodal generation, thus we exclude its generation related results from the table.

Method	Toke	nizer	Understanding			
112002100	LPIPS (↓)	PSNR(↑)	GQA (↑)	MME-P(↑)		
VQ-GAN-MLLM Slot-MLLM	0.3832 0.5559	13.80 12.14	47.7 58.1	777.2 1202.6		

C Slot-MLLM Analysis

C.1 Comparison with Patch-Level Tokenization

We conduct an ablation study comparing our proposed method against a simpler alternative that employs a patch-level tokenizer, specifically VQ-GAN [11]. The VQ-GAN tokenizer utilizes a discrete codebook of size 16,384, converting 256×256 images into discrete token sequences of size 16×16 .

As demonstrated in Table 10, Slot-MLLM significantly outperforms the model utilizing the patch-level VQ-GAN tokenizer. Conventional patch-based tokenization segments images into uniformly sized patches, primarily focusing on pixel-level reconstruction and encoding isolated visual features from individual patches. Although this enables VQ-GAN to achieve strong reconstruction performance compared to Slot Q-Former, VQ-GAN fails to effectively align visual representations with textual content. Consequently, it struggles in multimodal understanding and generation tasks due to its limited capability to capture detailed visual features and meaningful object-level context. In contrast, Slot Q-Former effectively captures rich visual context and object-level details while closely aligning these visual representations with textual content. This results in a substantial improvement in Slot-MLLM's ability to accurately interpret and generate detailed visual information. These findings highlight the importance of Slot Q-Former in achieving superior performance on multimodal tasks.

C.2 LLM Backbone Ablation

Our proposed Slot Q-Former can be easily integrated with various pretrained LLMs without requiring any architectural modifications. In this section, we additionally present experimental results using Qwen-2.5-14B-Instruct [76] and investigate the influence of the LLM backbone on overall performance. When training the Vicuna-7B [84] and Qwen-14B models, we use the same training datasets and settings, differing only in the LoRA rank. Additionally, to accommodate visual tokens, we expand the embedding layer of each LLM by 8192, equal to the codebook size. The detailed results are summarized in Table 11 for understanding benchmarks and Table 12 for generation benchmarks. Specifically, selecting superior base LLMs and larger model sizes leads to significantly enhanced

Table 11: Ablation study of Slot-MLLM with different LLM backbones on multimodal understanding benchmarks. * denotes a performance obtained by our own evaluation using the publicly available checkpoint. For all metrics, higher scores indicate better performance. The best scores among models are marked in **bold**.

Method LLM		COCO Caption	GQA	мме-р	SEED-Bench (Img)	POPE	MM-Vet	MMMU (val)	NaturalBench
SEED-LLaMA	Vicuna-7B	122.5*	52.4*	1123.9*	48.6*	78.0*	21.3*	26.8*	57.5*
Slot-MLLM-base	Vicuna-7B	119.39	53.8	1128.4	44.7	78.3	17.8	29	59.0
Slot-MLLM	Vicuna-7B	126.8	58.1	1202.6	47.4	79.8	20.6	28	60.5
Slot-MLLM	Qwen2.5-14B-Instruct	128.8	59.3	1239.4	54.4	82.4	24.9	46.2	66.8

Table 12: Ablation study of Slot-MLLM with different LLM backbones on text-to-image and editing benchmarks. * denotes a performance obtained by our own evaluation using the publicly available checkpoint. The best scores among models are marked in **bold**.

Method	Res.	Res. T2I-Compbe		ch(↑) Geneval(↑		GenAI-Bench(↑)		MagicBrush		EVR	
		color	shape	texture	(1)	Basic	Advanced	CLIP-I(↑)	L1 (↓)	CLIP-I(↑)	L1(↓)
SEED-LLaMA	768	0.1741*	0.2033*	0.2361*	0.29*	0.52*	0.49*	77.9*	28.8*	68.6*	31.1*
Slot-MLLM-base	768	0.1512	0.1766	0.2118	0.24	0.46	0.43	77.2	28.2	67.4	30.2
Slot-MLLM (7B)	256	0.2756	0.1990	0.2879	0.31	0.58	0.50	82.2	18.6	66.9	20.8
Slot-MLLM (14B)	256	0.2641	0.2204	0.2993	0.33	0.59	0.53	82.3	18.6	66.7	21.0

performance across both understanding and generation benchmarks, highlighting the benefits of scaling up the underlying LLM.

C.3 Qualitative Examples

We present qualitative examples of text-to-image generation by Slot-MLLM in Figure 6.

D Social Impacts

Broader Impacts. Our proposed Slot-MLLM advances multimodal understanding tasks and object-centric image generation, potentially facilitating more detailed, interactive, and integrated visual content creation, thus contributing significantly towards achieving more unified artificial general intelligence (AGI). However, as with many powerful generative models, Slot-MLLM could be misused for creating deceptive or harmful content such as misinformation or fake news. To address these potential negative impacts, we have included explicit guidelines for responsible model deployment and usage.

Safeguards. To mitigate potential risks associated with the misuse of Slot-MLLM, we have explicitly outlined guidelines for responsible usage, including ensuring ethical applications, careful validation of outputs, and transparent disclosure of AI-generated content. Upon public release, Slot-MLLM will be accompanied by these guidelines, alongside mechanisms enabling users to report issues, thus actively supporting responsible and accountable use of our multimodal generation technology.



Figure 6: Qualitative examples of text-to-image generation by Slot-MLLM